catalysts

MDPI

Article

Selective Alkylation of Benzene with Methanol to Toluene and Xylene over H-ZSM-5 Zeolites: Impact of Framework Al Spatial Distribution

Shu Ren [1,2], Fan Yang [2], Chao Tian [1], Yinghong Yue [1], Wei Zou [2], Weiming Hua [1,*] and Zi Gao [1]

[1] Shanghai Key Laboratory of Molecular Catalysis and Innovative Materials, Department of Chemistry, Fudan University, Shanghai 200438, China; 19110220067@fudan.edu.cn (S.R.); 21110220105@m.fudan.edu.cn (C.T.); yhyue@fudan.edu.cn (Y.Y.); zigao@fudan.edu.cn (Z.G.)

[2] State Key Laboratory of Green Chemical Engineering and Industrial Catalysis, SINOPEC Shanghai Research Institute of Petrochemical Technology Co., Ltd., Shanghai 201208, China; yangfan.sshy@sinopec.com (F.Y.); zouw.sshy@sinopec.com (W.Z.)

* Correspondence: wmhua@fudan.edu.cn; Tel.: +86-21-31249121

Abstract: The alkylation of benzene with methanol can effectively generate high-value-added toluene and xylene out of surplus benzene, which is now achieved primarily using solid acids like H-ZSM-5 zeolites as catalysts. In this work, two H-ZSM-5 samples with distinct framework aluminum (Al_F) distributions, but otherwise quite similar textural and acidic properties, have been prepared by employing tetrapropylammonium hydroxide (TPAOH) and *n*-butylamine (NBA) as organic structure-directing agents (OSDAs). Systematical investigations demonstrate that Al_F is preferentially located at the intersections in MFI topology when TPAOH is adopted. In contrast, less Al_F is positioned therein as NBA is utilized. Density functional theory (DFT) calculations reveal that the transition-state complexes cannot be formed in the straight and sinusoidal channels due to their much smaller sizes than the dynamic diameters of transition states, whereas there are adequate spaces for the formation of transition states at the intersections. Benefitting from abundant Al_F at the intersections, which provides more acid sites therein, H-ZSM-5 synthesized from TPAOH is more active relative to the counterpart obtained from NBA. At a WHSV of 4 h^{-1} and 400 °C, the former catalyst gives a 52.8% conversion, while the latter one affords a 45.9% conversion. Both catalysts display close total selectivity towards toluene and xylene (ca. 84%). This study provides an efficient way to regulate the distribution of acid sites, thereby enhancing the catalytic performance of H-ZSM-5 zeolite in the titled reaction.

Keywords: benzene alkylation; H-ZSM-5 zeolite; Al spatial distribution; DFT calculation

Citation: Ren, S.; Yang, F.; Tian, C.; Yue, Y.; Zou, W.; Hua, W.; Gao, Z. Selective Alkylation of Benzene with Methanol to Toluene and Xylene over H-ZSM-5 Zeolites: Impact of Framework Al Spatial Distribution. *Catalysts* **2023**, *13*, 1295. https://doi.org/10.3390/catal13091295

Academic Editors: De Fang and Yun Zheng

Received: 12 August 2023
Revised: 7 September 2023
Accepted: 11 September 2023
Published: 14 September 2023

1. Introduction

Benzene, toluene and xylene are very important chemical raw materials, which are extensively utilized in the production of organic solvents, gasoline octane number adjusting additives, vitamins and drugs [1–3]. In recent years, with the upgrading of gasoline quality, benzene, which was previously allowed to add into gasoline, has been greatly limited, resulting in a severe surplus, and concurrently, its price has witnessed a steep drop. However, the added values of toluene and xylene, as homologues of benzene, have kept growing steadily because of their reduced toxicity and wide usages in the manufacture of chemical intermediates, fine chemicals and polymers. Hence, the alkylation of benzene with methanol is a promising way to make better use of the surplus benzene, which has advantages such as mild operation conditions and an abundant source of methanol. This process can also seek a new way out for the current aromatic market [4–12].

It is generally accepted that benzene alkylation with methanol is catalyzed by Brønsted acid sites (BASs) from solid acid catalysts [13,14]; particularly, H-ZSM-5 zeolites are considered an excellent catalyst, owing to its unique acidity and pore structure. Previous research

has confirmed that the reaction can proceed via two mechanisms, namely the stepwise mechanism and the concert mechanism, according to both experimental and theoretical work [15,16]. In the stepwise mechanism (Figure S1), methanol is firstly adsorbed on a BAS to be protonated into $CH_3OH_2^+$, which is further dehydrated to obtain a methyl moiety bounced on the framework oxygen of the zeolite, i.e., the formation of surface-bonded methoxy group from methanol adsorption [17–20]. A benzene molecule then enters into the zeolite channel, which is adsorbed neighboring to the methoxy group. Thereafter, a methyl-benzene complex regarded as the transition state is encountered for the addition of the methoxy group to benzene [14,18]. A protonated toluene cation is subsequently attained when the energy barrier is overcome, whose back-donating a proton to the zeolite framework brings about the generation of a toluene molecule. For the concerted pathway (Figure S1), the dehydration of $CH_3OH_2^+$ and the attack from the methyl group on the benzene molecule simultaneously happen, leading to a transition state in the form of H_2O-CH_3-C_6H_6, while other elementary reactions are close to the stepwise ones [14,18]. It is rather difficult to quantitively distinguish the relative contributions of two mechanisms; consequently, the real reaction is possibly a combination of the above-mentioned two pathways. Apart from the main reaction, side reactions, including methanol to olefins (MTO), isomerization and methyl-transfer reaction, will also exist in the system, particularly for MTO, which gives rise to the generation of C_1–C_5 hydrocarbons and whose extent can be enhanced by higher acid density and sluggish diffusion [21].

It is generally considered that low acid density, hierarchical pores and small particle size of H-ZSM-5 zeolites are conducive to avoiding MTO reactions, reducing the by-product ethylbenzene (as a product via the alkylation of benzene with ethylene) and improving catalytic activity [8,22–24]. By far, properties including but not limited to morphology, Si/Al ratio and structure (core-shell, etc.) of the H-ZSM-5 zeolite have been deliberately explored to establish their relationships with the catalytic performances [8,25,26], yet there are other parameters of the H-ZSM-5 zeolite (surface area, crystal size, Al spatial distribution) that could exert significant influences on the catalytic behavior of H-ZSM-5 in the alkylation of benzene with methanol.

Numerous studies have shown that the distribution of Al atoms in the zeolite framework is not random but determined by the interaction between organic structural-directing agents (OSDAs) and zeolites [27–30]. Al sitting variations can be achieved by changing OSDAs, altering the gel composition, and adjusting the feeding sequence, etc. [30–36], which then determine the reaction path or carbon deposition rate, finally affecting the catalytic performance. Accordingly, Brønsted acid sites derived from framework aluminum (Al_F) of H-ZSM-5 can be divided into three types according to their exact locations, i.e., in the straight channels, sinusoidal channels and intersections. Although these three types of BASs can all be deemed as active sites, the adsorption enthalpy and entropy may be rather distinct due to the steric hindrances considering the different sizes between channels and intersections (5.1 × 5.5 Å for sinusoidal channels, 5.3 × 5.6 Å for straight channels and ca. 9 Å for intersection cavity). In particular, the steric constraints of bulky transition states can be more prominent for those acid sites located in the straight and sinusoidal channels. In consequence, previous reports have demonstrated significant differences in the catalytic performances of ethane and ethylene aromatization, MTO and 1-octene cracking reactions catalyzed by H-ZSM-5 with Al_F concentrated in intersections or channels [37–39]. Wang et al. found that the location of Al_F in H-ZSM-5 could influence catalytic performance in the alkylation of benzene with methanol, and they attributed this phenomenon to the co-adsorption effect of benzene and methanol when Al_F was located at intersections [40]. However, the chemical environment of Al_F at different locations is also believed to be capable of altering the host–guest interaction between the transition state and the H-ZSM-5 zeolite framework, thus determining catalytic properties. On the one hand, the implementation of the above catalyst preparation will often introduce other variables aside from the aluminum location, thereby affecting the accuracy of the results. On the other hand, the

function of Al sittings on the catalytic performance of H-ZSM-5 in the alkylation of benzene with methanol is still far from sufficient understanding.

In this work, to study the influence of Al_F distribution on benzene alkylation with methanol from a mechanistic perspective, two H-ZSM-5 samples possessing very similar textural and acidic properties were synthesized utilizing tetrapropylammonium hydroxide and *n*-butylamine as OSDAs (i.e., templates). This work unveils that the acid sites (derived from Al_F) located in the straight and sinusoidal channels are not as active as those at the intersections due to a confined effect, i.e., the smaller spaces of the channels on the transition states as demonstrated by DFT calculations, which provides a new insight into the structure–activity relationship on the titled reaction.

2. Results and Discussion

2.1. Structural and Textural Properties

As shown in Figure 1, XRD patterns of both Z5-NBA and Z5-TPA exhibit typical diffraction peaks at 8.0°, 8.9°, 9.1°, 23.1°, 23.3°, 23.7°, 24.0° and 24.4° out of the (101), (020), (111), (332), (051), (151), (303) and (133) crystal planes in MFI topology (PDF #44-0003), respectively, indicating the successful formation of the H-ZSM-5 zeolite without detectable impurities [41,42]. The relative crystallinity was calculated by integrating the areas of diffraction peaks within 22.5−25°, and the sum of the areas for Z5-NBA was set as 100% for reference. As listed in Table 1, the XRD crystallinity of Z5-TPA and Z5-NBA was 105% and 100%, respectively. The close crystallinity suggests that both TPA^+ and NBA OSDAs are capable of generating H-ZSM-5 zeolites with high crystallinity.

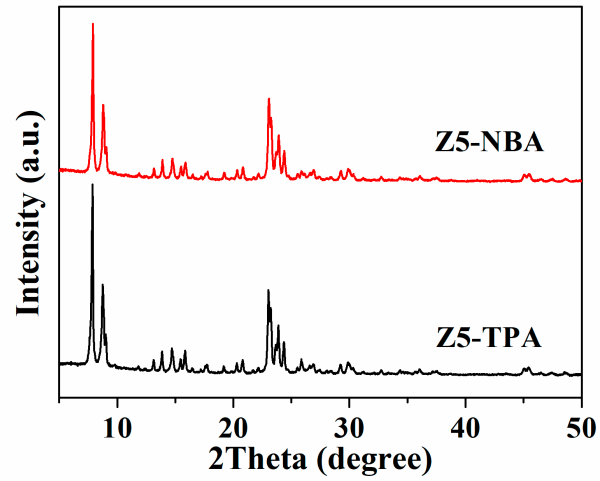

Figure 1. XRD patterns of Z5-TPA and Z5-NBA.

Table 1. Textural properties of Z5-TPA and Z5-NBA.

Sample	Si/Al Ratio [a]	Crystallinity (%)	Surface Area (m^2/g)		Pore Volume (cm^3/g)	
			Total	Micro [b]	Micro [b]	Meso [c]
Z5-TPA	151	105	398	361	0.17	0.10
Z5-NBA	149	100	393	358	0.17	0.10

[a] Determined by XRF; [b] Micropore volume calculated by the *t*-plot method; [c] Mesopore volume.

The SEM images for Z5-TPA and Z5-NBA are displayed in Figure 2. Both Z5-TPA and Z5-NBA zeolites are composed of spherical particles with diameters of around 3 μm for Z5-TPA and 2.6 μm for Z5-NBA (Figure 2a,c). The high-resolution micrographs (Figure 2b,d) evidence that the two samples are constructed by strip-like crystals of ~350 nm in length and ~100 nm in width for Z5-TPA and ~460 nm in length and ~120 nm in width for Z5-NBA

with smooth surfaces. The SEM result demonstrates that both Z5-TPA and Z5-NBA zeolites have the same morphology and similar particle and crystal sizes.

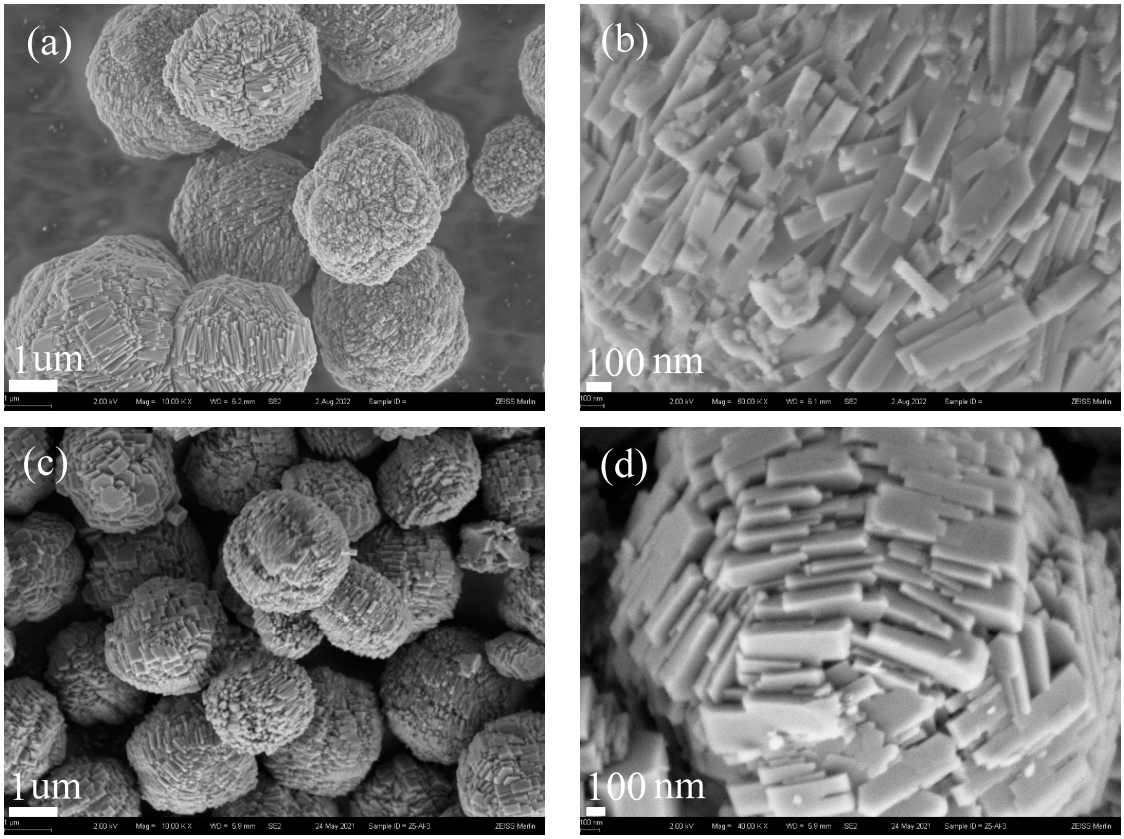

Figure 2. SEM graphs of Z5-TPA (**a**,**b**) and Z5-NBA (**c**,**d**).

As shown in Table 1, both Z5-TPA and Z5-NBA samples possess similar BET surface areas (ca. 395 m^2/g) and micropore surface areas (ca. 360 m^2/g). The total pore volumes (0.27 cm^3/g) and micropore volumes (0.17 cm^3/g) are the same for both samples. The Si/Al molar ratios measured by XRF are close for both zeolites (151 vs. 149), which are equivalent to those of the initial gels (150). These observations confirm that both Z5-TPA and Z5-NBA display very similar textural properties and chemical compositions.

2.2. Acidic Properties

Acidity is an important property of zeolites, which is directly related to the Si/Al ratio. The surface acidity of H-ZSM-5 samples was determined by NH_3-TPD (Figure 3). As shown on the NH_3-TPD curves, both Z5-TPA and Z5-NBA have two distinctive desorption peaks at 185 °C and 376 °C, which are attributed to the desorption of NH_3 molecules that interact with the weak acids and strong acids, respectively [43,44]. Judging from the peak temperature, the acid strength of Z5-TPA is the same as that of Z5-NBA. The quantitative results listed in Table 2 indicate that both Z5-TPA and Z5-NBA possess quite similar amounts of weak acid sites (59 vs. 60 μmol/g), strong acid sites (70 vs. 70 μmol/g) and total acid sites (129 vs. 130 μmol/g). This finding is a consequence of the close Si/Al ratio for two samples.

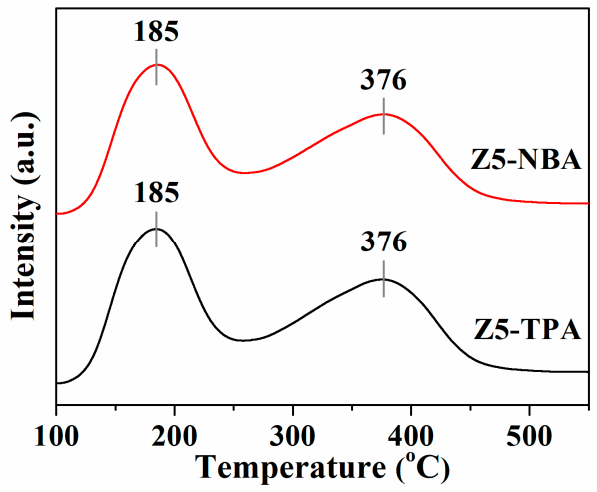

Figure 3. NH_3-TPD profiles of Z5-TPA and Z5-NBA.

Table 2. Acidic properties of Z5-TPA and Z5-NBA.

Sample	Acidity by NH_3-TPD (μmol/g)			Acidity by Py-IR (μmol/g)			BAS Distribution (%) [a]			Conv. of Cumene Cracking (%)
	Weak	Strong	Total	Brønsted	Lewis	Total	Weak	Medium	Strong	
Z5-TPA	59	70	129	78	17	95	22	31	47	33.9
Z5-NBA	60	70	130	78	17	95	22	31	47	33.6

[a] The acid strength distribution of Brønsted acid sites (BASs) was estimated from Py-IR after the evacuation at different temperatures; the difference in BAS between 200 and 300 °C, the difference in BAS between 300 and 400 °C and the remaining BAS at 400 °C correspond to weak, medium and strong acid sites, respectively.

Considering that NH_3-TPD cannot distinguish the type of acid sites, Py-IR experiments were also carried out to determine the amounts of Brønsted acid sites (BASs) and Lewis acid sites (LASs), as well as the distribution of Brønsted acid strength. On the Py-IR spectra (Figure 4), the peak at 1455 cm^{-1} is attributed to pyridine adsorbed on LASs, whereas the 1541 cm^{-1} band is assigned to pyridine adsorbed on BASs [45,46]. Furthermore, the peak at 1489 cm^{-1} is caused by pyridine adsorbed on both BASs and LASs [47]. The quantitative results are summarized in Table 2, in which the total acidity is measured at 200 °C. For the two samples, the amounts of BAS and LAS are the same. Brønsted acid sites account for the majority of the overall acid sites with a ratio of Brønsted acidity to Lewis acidity of 4.6. Moreover, the proportions of weak, medium and strong BAS amounts among the total Brønsted acidity are the same for both Z5-TPA and Z5-NBA samples, indicating that they have the same distribution across the Brønsted acid strength.

Cumene cracking is a typical reaction catalyzed by Brønsted acid sites [48,49]. As shown in Table 2, the cumene conversion over the two samples is very close, which is 33.9% for Z5-TPA and 33.6% for Z5-NBA. This observation demonstrates very similar Brønsted acidity of the two samples, which is consistent with the result of Py-IR. The above results demonstrate that both Z5-TPA and Z5-NBA display very close acidic properties, including the acid amount, acid strength, acid type and the strength distribution of BAS.

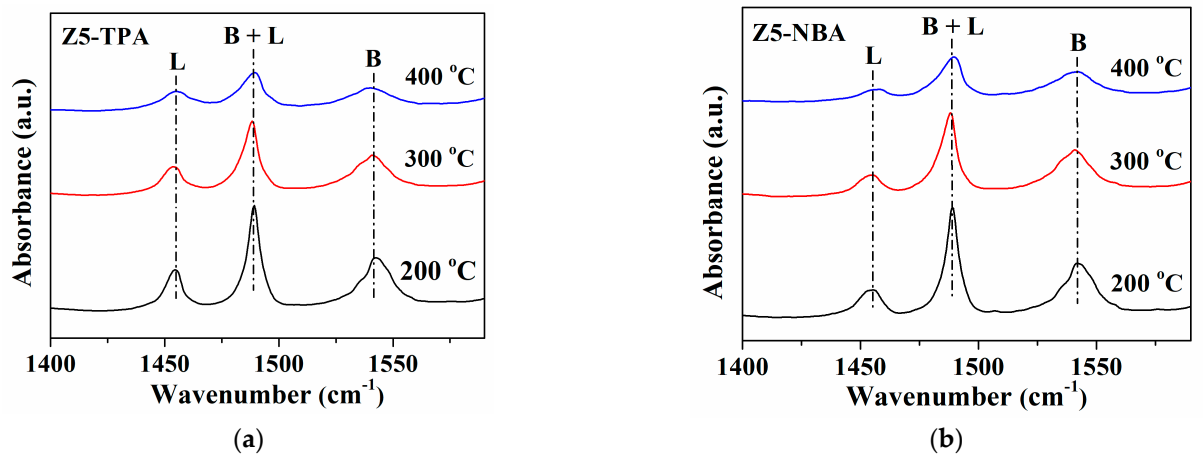

Figure 4. Py-IR spectra of (**a**) Z5-TPA and (**b**) Z5-NBA after desorption at 200 °C, 300 °C and 400 °C.

2.3. ^{29}Si and ^{27}Al MAS NMR, Constraint Index

As the textural properties, composition, morphology and acidic properties of Z5-NBA and Z5-TPA are almost identical, solid-state MAS NMR measurements were carried out to investigate the chemical environments of Si and Al. The ^{29}Si MAS NMR spectra illustrated in Figure 5 show closely similar features, and four sub-peaks are fitted from the origin curve at approximately −103, −107, −113 and −116 ppm, respectively. Two peaks of −113 and −116 ppm are attributed to symmetric and slightly asymmetric $Q^4(0Al) = Si(OSi)_4$-type silicon connecting to four Si tetrahedrons in the H-ZSM-5 framework [37,50]. The peak at −107 ppm in the fitting curve is assigned to $Q^4(1Al) = Si(OSi)_3(OAl)$-type silicon linking to one Al tetrahedron and three Si tetrahedrons in the H-ZSM-5 framework [51–53]. The peak centered at −103 ppm is associated with $Q^3(0Al) = Si(OSi)_3(OH)$-type silicon connecting to three Si tetrahedrons in the zeolite framework and one hydroxyl, which is located on the surface of H-ZSM-5 [27,37,54]. The quantitative results given in Table 3 show close relative proportions of various Si species for Z5-TPA and Z5-NBA, revealing that both zeolites have quite similar SiO_4 environments.

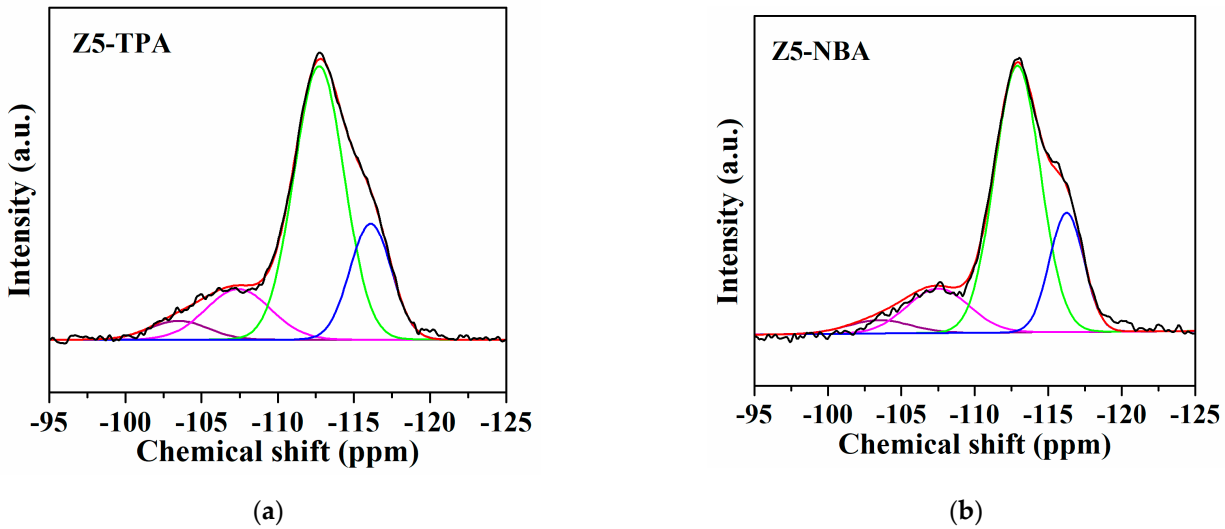

Figure 5. ^{29}Si MAS NMR spectra of (**a**) Z5-TPA and (**b**) Z5-NBA.

Table 3. Deconvolution results of the ^{29}Si MAS NMR spectra for Z5-TPA and Z5-NBA based on the normalized peak areas of different Si species.

Sample	Proportion of Various Peaks (%)			
	Q^3(0Al), −103 ppm	**Q^4(1Al), −107 ppm**	**Q^4(0Al), −113 ppm**	**Q^4(0Al), −116 ppm**
Z5-TPA	4.7	14.4	60.1	20.8
Z5-NBA	4.6	14.5	60.4	20.5

In the ^{27}Al MAS NMR spectra, as shown in Figure 6a, both Z5-TPA and Z5-NBA samples exhibit one intense resonance peak at 55 ppm corresponding to tetrahedrally coordinated Al species, while the resonance signal at 0 ppm attributed to octahedrally coordinated extra-framework Al species is almost invisible, corroborating that the great majority of Al atoms have been incorporated into the H-ZSM-5 zeolite framework [37,55–58]. The ^{27}Al MAS NMR spectrum at 55 ppm is deconvolved into five peaks located at 48, 52, 55, 57 and 60 ppm, respectively, as illustrated in Figure 6b,c. The peaks centered at 48, 52 and 55 ppm can be assigned to the framework Al atoms at the intersections, whereas the peaks at 57 and 60 ppm correspond to framework Al atoms in the sinusoidal and straight channels of the H-ZSM-5 zeolite, respectively [38]. The framework aluminum distribution was then calculated based on the proportion of various peak areas, and the results are presented in Table 4. The relative content of Al at the intersections is obviously higher for Z5-TPA (86.4%) than Z5-NBA (69.0%), while the former sample has noticeably lower content of Al in the sinusoidal channels than the latter one (9.9% vs. 25.7%). This result suggests that Al_F is more favored to be positioned at the intersections when TPA^+ was employed as OSDA.

Table 4. Aluminum distribution obtained from the curve fitting of ^{27}Al MAS NMR spectra and CI values for C_6 paraffins cracking over Z5-TPA and Z5-NBA.

Sample	Aluminum Distribution (%)			CI [a]
	Straight	**Sinusoidal**	**Intersection**	
Z5-TPA	3.7	9.9	86.4	3.4
Z5-NBA	5.3	25.7	69.0	5.0

[a] Constraint index.

Notably, during the synthesis of aluminosilicate zeolites, the isomorphic substitution of framework Si^{4+} by Al^{3+} leads to the formation of negative charges, which must be balanced with positively charged species; these species could be OSDAs (e.g., TPA^+, hydrolyzed and dissociated amines), extra-framework Al species (e.g., AlO^+, $Al(OH)^{2+}$) and inorganic cations (e.g., Na^+, K^+) [28]. To guarantee a neutral framework and the continuation of crystallization, the framework Al atoms will be located near positions that are more suitable for the accommodation of the above-mentioned cations. In the classical crystallization mechanism of the ZSM-5 zeolite, when the large-sized TPA^+ was used as OSDA, it can only be located at the intersections with larger void spaces [37,59], which leads to the enrichment of Al_F at the intersections. Z5-NBA is obtained with the assistance of NBA and Na^+, both of which are small-sized and will be randomly distributed within the MFI framework during the crystallization process, resulting in less framework Al atoms distributed at the intersections than Z5-TPA. The difference in Al_F location is further demonstrated by the following constraint index.

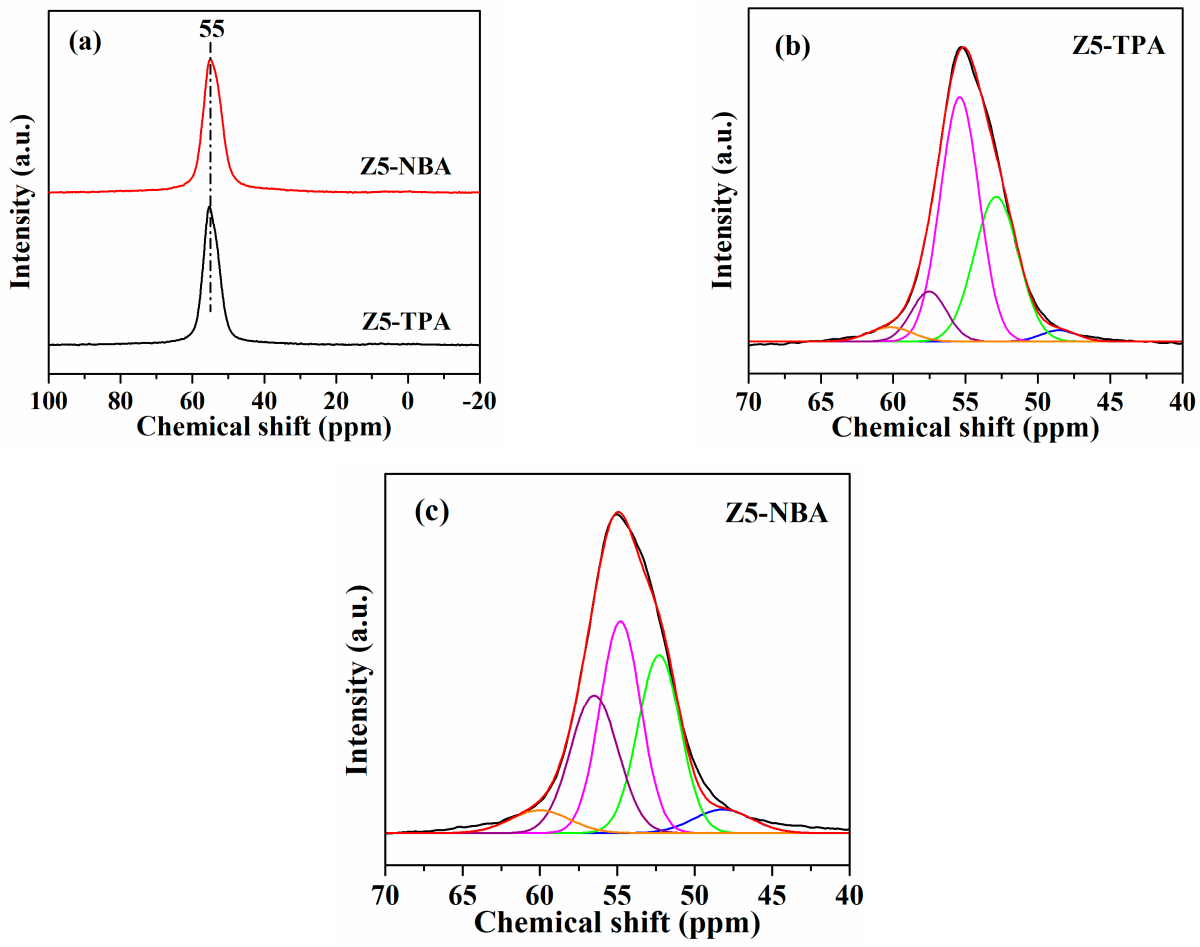

Figure 6. ^{27}Al MAS NMR spectra of Z5-TPA and Z5-NBA (**a**) and their corresponding curve fittings of Z5-TPA (**b**) and Z5-NBA (**c**).

The constraint index (CI) is used to estimate the distribution of acid sites derived from the framework Al atoms. The CI value is determined from the cleavage rate ratio of *n*-hexane to 3-methylpentane, which was measured at a conversion rate below 15%. Considering that both Z5-TPA and Z5-NBA zeolites have an identical MFI structure and quite similar textural and acidic properties, the variation in the CI value can be attributed to the difference in the distribution of framework Al atoms. The CI values of H-ZSM-5 zeolites synthesized with different OSDAs are shown in Table 4. The CI value of Z5-NBA is higher than that of Z5-TPA (5.0 vs. 3.4). This result suggests that the amount of acid sites at the intersections is greater for Z5-TPA than Z5-NBA, since the cracking reaction of 3-methylpentane proceeds faster at the intersections than in the straight and sinusoidal channels due to the larger spaces of intersections that can accommodate the bulky bimolecular transition state [28]. Combined with the ^{27}Al NMR result, it is clear that the preferential positioning of TPA^+ at the intersections causes more framework Al atoms to sit therein, leading to more acid sites concentrated at the intersections. Compared to Z5-TPA, the Z5-NBA sample attained from NBA and Na^+ displays less framework Al atoms and acid sites at the intersections, i.e., more framework Al atoms and acid sites in the straight and sinusoidal channels.

2.4. Catalytic Performance

The selective alkylation of benzene with methanol to toluene and xylene is catalyzed by Brønsted acid sites of the zeolites derived from Al_F [13,14]. We compared catalytic behavior of Z5-TPA and Z5-NBA to investigate the effect of Al_F distribution. The reaction

data after 4 h on stream given in Table 5 shows that the total selectivity towards toluene and xylene is very close for the two samples, which is 84.4% and 84.0% for Z5-TPA and Z5-NBA, respectively. However, the benzene conversion of Z5-TPA (52.8%) is noticeably higher than that of Z5-NBA (45.9%), and a higher total yield of toluene and xylene is also observed over Z5-TPA (44.6%) compared to Z5-NBA (38.6%). In terms of reaction rate, Z5-TPA displays a much higher rate than Z5-NBA (2445 vs. 1510 mmol/(g h)). The catalytic activity strongly depends on Brønsted acid properties of the zeolites, i.e., amount, strength and distribution [60]. Larger surface area provides more accessible acid sites in the zeolites, resulting in higher conversion of benzene. Hu et al. found that introducing mesopores in H-ZSM-5 could improve benzene conversion, due to enhanced diffusion of reactants and products, as well as easier access to the active sites in micropores [23]. The aforementioned characterization results reveal that both Z5-TPA and Z5-NBA zeolites have the same mesopores, very similar surface areas and very close acidic properties, including amount, strength, and strength distribution of the BAS. Therefore, the difference in catalytic activity should be attributed to the distribution of acid sites, i.e., the Al_F distribution.

Table 5. Reaction data of the Z5-TPA and Z5-NBA catalysts at a WHSV of 4 h^{-1} and 400 °C.

Catalyst	Conversion	Selectivity (%) [a]						S_{T+X} [b]	Y_{T+X} [c]	Rate [d]
	(%)	T	PX	MX	OX	EB	C_{9+}	(%)	(%)	(mmol/(g h))
Z5-TPA	52.8	52.4	8.7	16.5	6.8	10.5	5.1	84.4	44.6	2445
Z5-NBA	45.9	48.5	9.2	18.1	8.2	7.3	8.7	84.0	38.6	1510

[a] T: toluene; PX: *p*-xylene; MX: *m*-xylene; OX: *o*-xylene; EB: ethylbenzene; C_{9+}: trimethylbenzene and higher alkyl aromatics. [b] S_{T+X} refers to the total selectivity of toluene and xylene. [c] Y_{T+X} refers to the total yield of toluene and xylene. [d] Millimoles of benzene converted per gram of catalyst per hour at 400 °C obtained at a benzene conversion below 10%.

The apparent activation energies in the temperature range of 375−450 °C were measured for Z5-TPA and Z5-NBA. As illustrated in Figure 7, both zeolites have equivalent activation energies (90 vs. 89 kJ/mol), suggesting that the reaction mechanism on these catalysts is the same.

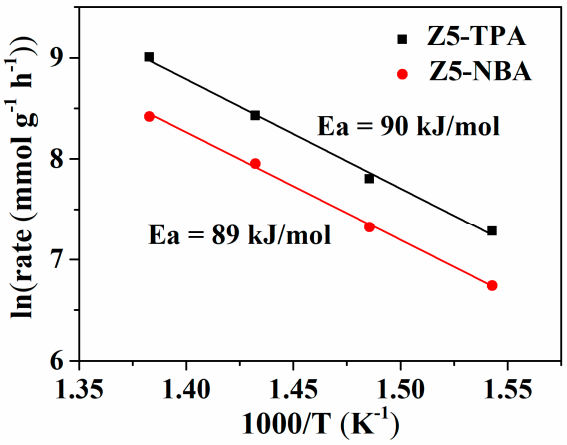

Figure 7. Arrhenius plot of the reaction rate on Z5-TPA and Z5-NBA.

Spectroscopic studies have verified that methoxy groups may indeed be formed from methanol, which is in accordance with a stepwise mechanism [15,60]. On the other hand, some reports favor the concerted mechanism [61,62]. Quantum chemical calculations have demonstrated the possibility of both mechanisms [16]. We think that both routes may exist during the reaction.

2.5. Periodic Density Functional Study

According to the above analysis, the only difference between Z5-NBA and Z5-TPA lies in the location of Al_F, which determines the sittings of active centers, i.e., the acid sites. To understand the link between the Al_F location and reaction mechanism, a periodic density functional study was conducted using the Vienna Ab-initio Simulation Package (VASP 4.6).

Firstly, the small size of NBA makes straight channels, sinusoidal channels and channel intersections all feasible locations for its existence, and the adsorption energies of NBA at the three locations are all close to −1.47 eV. Both the configurations and energies for NBA in ZSM-5 concrete the regular dispersion of NBA in ZSM-5; meanwhile, given that NBA can be positively charged after hydrolyzation and dissociation, a more even distribution of Al_F at the three locations can be anticipated. More importantly, the addition of Na^+ cations, which are randomly distributed in the MFI framework, also contributes significantly to the uniform dispersion of Al_F in Z5-NBA [37]. Different from NBA, it has been found that TPA^+ could only be resided at the intersections due to its large size, with an adsorption energy of −4.18 eV. Considering the fact that no other cations can be found in the synthesis of Z5-TPA, Al_F will be directed into the channel intersections of ZSM-5 zeolite via the charge interaction between TPA^+ and AlO_4^-. The simulations are consistent with the ^{27}Al MAS NMR and CI results, which further corroborates that the Al_F is more concentrated at the intersections for Z5-TPA than Z5-NBA.

Since the acid sites come from the compensating protons adjacent to Al_F, various Al_F locations bring about simultaneous changes in the coordinates of acid sites. Specifically, the acid sites in the straight/sinusoidal channels face confined spaces, yet the acid sites in the cross-sections (i.e., channel intersections) hold more spacious room. As mentioned in the introduction, two possible mechanisms are involved in the alkylation of benzene with methanol, namely the concerted pathway and the stepwise pathway, and the largest intermediates in the two processes are believed to be transition-state complexes before the generation of protonated toluene cations. Theoretically, the configurations of transition-state complexes could exist in the channels or intersections; however, unluckily, only those at the intersections can be found after searching for a series of potential models no matter how these precursors are placed, and to the best of our knowledge, no evidence has been found to support the formation of transition states in the straight and sinusoidal channels. In the determined configuration of the concerted pathway, an oxygen atom in the water, a carbon atom in the methyl and a carbon atom in the benzene are aligned almost linearly, with the angle of 171.8°, C-O length of 2.2 Å and C-C length of 2.1 Å (Figure 8). Similarly, in the determined configuration of the stepwise pathway, a framework oxygen atom, a carbon atom in the methyl and a carbon atom in the benzene are also linearly arranged, with C-O distance of 2.2 Å, C-C distance of 2.1 Å and O-C-C angle of 178.0° (Figure 9). Accordingly, the dynamic diameters of the two transition-state complexes are calculated using the method put forward by Mehio et al. [63], which is 7.3 Å for the stepwise pathway and 9.1 Å for concerted pathway. Obviously, the kinetic diameters are much larger than the sizes of ZSM-5 apertures (5.1 × 5.5 Å for sinusoidal channels and 5.3 × 5.6 Å for straight channels). Consequently, there are insufficient spaces for the formation of transition states in the straight and sinusoidal channels, which hinders the proceeding of the alkylation reaction.

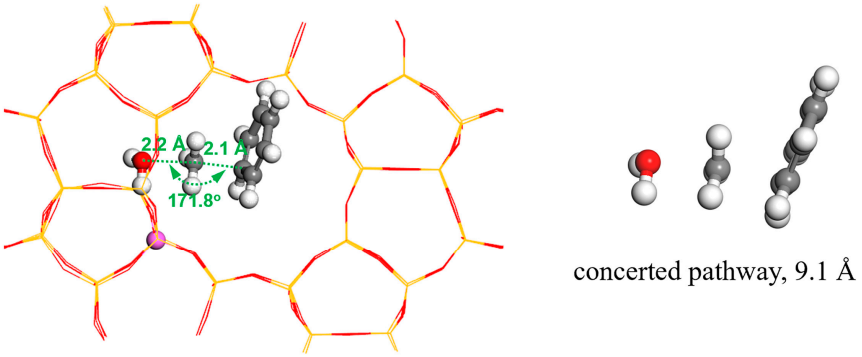

Figure 8. The transition-state complex in the optimized geometry by the concerted mechanism (red, oxygen; purple, aluminum; white, hydrogen; gray, carbon; similarly hereinafter).

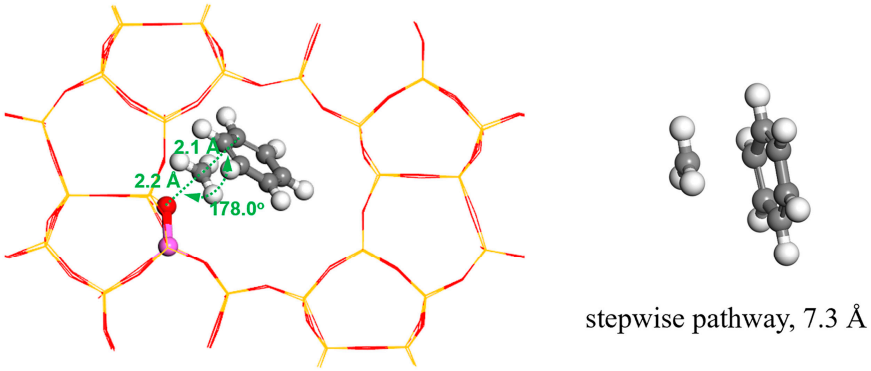

Figure 9. The transition-state complex in the optimized geometry by the stepwise mechanism.

Liu et al. [37] reported that Pt-modified ZSM-5 with acid sites mainly located in the intersections tended to produce more aromatic compounds for ethane aromatization than a catalyst with acid sites located in the straight and/or sinusoidal channels. The reason for this is that acid sites located in the intersections with more space void were conducive for the geometry transformation of intermediates. Zhu et al. [40] studied the effect of Al_F distribution on the catalytic performance in the alkylation of benzene with methanol. The results demonstrated that H-ZSM-5 with more Al_F in the intersections can improve benzene conversion due to the larger space and co-adsorption effect. Taken everything into consideration, in the synthesis of ZSM-5, TPA^+ will be only located at the intersections, which causes the preferential enrichment of Al_F as well as acid sites therein. As there are larger spaces near to the acid sites at the intersections, the alkylation of benzene with methanol could progress smoothly, pertaining to the minimized steric hindrances for the large transition-state complexes. Compared to TPA^+, the engagement of NBA and Na^+ induces more acid sites present in the straight and sinusoidal channels. However, these channel acid sites are incapable of catalyzing the alkylation reaction because of the narrow spaces which could not hold the large transition-state complexes. Resultantly, Z5-TPA displays higher activity than Z5-NBA in the alkylation of benzene with methanol attributing to the rational Al_F locations.

3. Materials and Methods

3.1. Synthesis of H-ZSM-5 Zeolites

Two ZSM-5 zeolites were synthesized using the procedures described by Liu et al. with minor modifications [37]. Typically, silica sol (SiO_2, 40 wt%) was added slowly to $Al(NO_3)_3$ aqueous solution, and stirred for 1 h. Then, tetrapropylammonium hydroxide (TPAOH, 40 wt%) was added, followed by stirring for 4 h to form a homogeneous suspension with a molar composition of 1.0 SiO_2:0.00333 Al_2O_3:0.5 TPAOH:50 H_2O. The suspension was

transferred into a Teflon-lined stainless-steel autoclave and statically crystallized at 170 °C for 120 h, followed by centrifuging, rinsing, drying overnight at 120 °C and calcining at 550 °C in air for 5 h.

Another ZSM-5 zeolite was prepared as follows: silica sol was added slowly to the mixed aqueous solution containing $Al(NO_3)_3$ and NaOH. Then, *n*-butylamine (NBA) was added, followed by stirring for 4 h to obtain a gel with a molar composition of 1.0 SiO_2:0.00333 Al_2O_3:0.98 NBA:0.08 Na_2O:10 H_2O. The prepared mother gel was transferred into a Teflon-lined stainless-steel autoclave and crystallized at 170 °C for 120 h, followed by centrifuging, rinsing, drying overnight at 120 °C and calcining at 550 °C in air for 5 h.

The NH_4-type zeolites were obtained by ion-exchanging the above ZSM-5 zeolites with 1 M NH_4NO_3 solution three times with a solution/zeolite ratio of 10 mL/g at 90 °C for a total of 9 h. The H-type ZSM-5 samples were acquired by calcination of the NH_4-type zeolites at 450 °C for 5 h. The resulting H-ZSM-5 catalysts were denoted as Z5-TPA and Z5-NBA, respectively.

3.2. Characterization of H-ZSM-5 Zeolites

Zeolite topologies were determined from powder X-ray diffraction (XRD) patterns on a D8 Advance X-ray diffractometer (Brucker, Madison, WI, USA) with a Cu Kα radiation source at 40 kV and 50 mA. Scanning electron microscopy (SEM) images of the samples were observed on a Zeiss Merlin scanning electron microscope (Merlin, Carl Zeiss AG, Oberkochen, Germany). The Si/Al molar ratios of H-ZSM-5 zeolites were determined by means of an S4 Pioneer X-ray fluorescence (XRF) spectrometer (Bruker, Rheinstetten, Germany). The surface areas and pore volumes of H-ZSM-5 zeolites were measured by a Micromeritics TriStar 3000 automatic absorption instrument (Micromeritics, Atlanta, GA, USA). Magic-angle-spinning nuclear-magnetic-resonance (MAS NMR) spectra of ^{27}Al and ^{29}Si were collected on a Bruker Avance III 600 MHz Wide Bore spectrometer (Bruker, Rheinstetten, Germany). The single-pulse sequence was adopted with a 10° pulse and a delay time of 0.3 s. The chemical shifts for ^{27}Al and ^{29}Si were calibrated by referring to $AlCl_3$ and tetramethylsilane, respectively. The ^{27}Al MAS NMR and ^{29}Si MAS NMR spectra were deconvoluted by using the mixed Gaussian–Lorentzian equation.

The strength and quantity of acid sites present on H-ZSM-5 zeolites were analyzed by temperature-programmed desorption of NH_3 (NH_3-TPD) on a Micrometritics AutoChem AMI-3300 apparatus (Micromeritics, Atlanta, GA, USA). A total of 0.1 g of sample (40−60 mesh) was loaded into a U-type tube and pretreated at 550 °C for 1 h in a N_2 flow. Then, the sample was cooled to 100 °C and exposed to a 10 vol.% NH_3/N_2 mixture (30 mL/min) for 0.5 h. After purging with helium (30 mL/min) for an additional 2 h to remove the physically adsorbed NH_3, the temperature was ramped from 100 °C to 550 °C at a rate of 10 °C/min using helium (30 mL/min) as the carrier gas. The desorbed ammonia was monitored by a thermal conductivity detector. The amounts of Brønsted and Lewis acid sites were determined by Fourier-transform infrared spectroscopy of pyridine adsorption (Py-IR) on a Nicolet iS50 spectrometer (Nicolet, Madison, WI, USA). Prior to each measurement, all samples were pressed into self-support wafers with a diameter of 13 mm and a weight of ca. 15 mg. Then, the sample was degassed at 400 °C for 2 h under vacuum ($<10^{-2}$ Pa) to remove the impurities and adsorbed water, before being cooled to an ambient temperature. Thereafter, pyridine was introduced into the testing cell as saturated vapor for 10 min to allow sufficient adsorption, after which the cell was evacuated again for 20 min at 200 °C, 300 °C and 400 °C. The spectra were recorded using the background taken at the same temperature. Brønsted and Lewis acidities were quantified from the integrated areas of Py-IR bands at ca. 1540 and 1450 cm^{-1}, employing the molar extinction coefficients of 1.67 and 2.22 cm/μmol, respectively [64,65].

3.3. Computational Method

Density functional theory (DFT) calculations were carried out using Vienna Ab Initio Simulation Package 5.4. Project augmented wave method and Perdew–Burke–Ernzerhof

exchange–correlation function were adopted, with a plane wave basis set kinetic energy cut-off of 400 eV. The Brillouin zone sampling was limited to the Γ-point, and the convergence criterion that forces on each atom was smaller than 0.03 eV/Å. The MFI structure containing pure SiO_2 was downloaded from International Zeolite Association, whose lattice parameters were then optimized to acquire a unit cell of a = 20.32 Å, b = 20.16 Å and c = 13.46 Å. A Brønsted acid site was created by replacing a Si (T12) atom with an Al atom, and the neighboring O between Al (T12) and Si (T3) was protonated. The dimer method was utilized to determine the transition states. The obtained configurations were confirmed by the existence of one and the only imaginary frequency. The adsorption energy was calculated by the following equation:

$$\Delta E_{ads} = E_{zeo+temp} - E_{zeo} - E_{temp} \quad (1)$$

wherein ΔE_{ads} is the adsorption energy, $E_{zeo+temp}$ is the total energy of zeolite and template complexes, and E_{zeo} and E_{temp} are the energies of the zeolite framework and the template, respectively.

3.4. Catalytic Performace Evaluation

3.4.1. Estimation of Constraint Index

A total of 0.2 g of the catalyst (40−60 mesh) was loaded into the constant temperature zone of the fixed bed reactor. Prior to each test, the H-ZSM-5 zeolite was firstly activated at 450 °C for 3 h in a N_2 flow, and the temperature was cooled to 400 °C. Next, a mixed feedstock of *n*-hexane and 3-methylpentane with a molar ratio of 1:1 was pumped into the reactor using N_2 as the carrier gas to ensure a C_6 paraffin conversion below 15%. The reactor effluent was analyzed online by a gas chromatograph equipped with a flame ionization detector and a HP-PLOT Q capillary column (30 m × 0.32 mm × 20 μm). The constraint index (CI) value was calculated by the following equation [66]:

$$\text{constraint index} = \frac{\log(\text{fraction of n-hexane remaining})}{\log(\text{fraction of } 3-\text{methylpentane remaining})} \quad (2)$$

3.4.2. Benzene Alkylation with Methanol

The alkylation of benzene with methanol was carried out in a fixed bed reactor. The catalyst (3 g, 20−40 mesh) was loaded into the thermostatic region of the reactor and pretreated at 450 °C for 3 h in a N_2 flow. Then, the temperature was cooled to 400 °C. Next, a mixture of benzene/methanol as the reactant (molar ratio of 1:1) was pumped in the reactor with a co-feed N_2 flow (50 mL/min). The weight hourly space velocity (WHSV) was 4.0 h^{-1}. The products were analyzed offline by a gas chromatograph equipped with a flame ionization detector and a HP-INNOWAX capillary column (50 m × 0.32 mm × 0.5 μm).

3.4.3. Cumene Cracking

The cracking reaction of cumene was used to evaluate Brønsted acidity of H-ZSM-5 zeolites, which was carried at 300 °C in a pulsed microreactor loaded with 0.03 g of the catalyst (40−60 mesh). The catalyst was activated at 450 °C for 3 h in a He flow before reaction. The carrier gas was He (30 mL/min), and the amount of injected cumene was 1 μL.

4. Conclusions

In this work, two micron-sized spherical H-ZSM-5 zeolites with very similar surface areas, SiO_4 environments, acidic properties comprising the acid amount, acid strength, acid type and the strength distribution of BAS, but different Al_F distributions, were synthesized by using TPAOH and NBA as OSDAs, respectively. When the large-sized TPA^+ cations that could only be located at the intersections with larger void spaces are used, Al_F is preferentially concentrated at the intersections. In contrast, the random existence of the small-sized NBA and Na^+ in the MFI framework during the crystallization process leads to less Al_F

distributed at the intersections. DFT calculations unveil that the Al_F at the intersections exerts less steric hindrances for the transition states, whereas there are insufficient spaces for the formation of transition states in the straight and sinusoidal channels, which hinders the proceeding of the alkylation reaction. The Z5-TPA zeolite synthesized from TPAOH gives a 52.8% conversion in benzene alkylation with methanol at a WHSV of 4 h^{-1} and 400 °C, which is more active than the Z5-NBA zeolite synthesized from NBA (45.9% conversion). The comparable total selectivity towards toluene and xylene (ca. 84%) was achieved over both H-ZSM-5 zeolites. The higher activity observed for Z5-TPA than Z5-NBA is attributed to more Al_F distributed at the intersections of the former catalyst, i.e., more Brønsted acid sites located therein. This work not only provides a feasible method to control the Al distribution in the H-ZSM-5 zeolite framework, thus improving the catalytic performance in the titled reaction, but is also helpful in understanding the structure–performance relationship.

Supplementary Materials: The following supporting information can be downloaded at: https://www.mdpi.com/article/10.3390/catal13091295/s1, Figure S1: Schematic representation of the stepwise (middle and bottom row) and concerted mechanism (top row) for benzene alkylation with methanol on H-ZSM-5 zeolite.

Author Contributions: S.R.: investigation, data curation, writing—original draft. F.Y.: methodology, writing—original draft. C.T.: investigation, data curation. Y.Y.: methodology, formal analysis. W.Z.: methodology, formal analysis. W.H.: conceptualization, supervision, writing—review and editing, project administration. Z.G.: validation, formal analysis. All authors have read and agreed to the published version of the manuscript.

Funding: This work was financially supported by the National Natural Science Foundation of China, grant number 22072027, the Science and Technology Commission of Shanghai Municipality, grant number 19DZ2270100 and SINOPEC Shanghai Research Institute of Petrochemical Technology Co., Ltd., grant number 33750000-19-ZC0607-0005.

Data Availability Statement: Not applicable.

Conflicts of Interest: The authors declare no conflict of interest.

References

1. Ahn, J.H.; Kolvenbach, R.; Al-Khattaf, S.S.; Jentys, A.; Lercher, J.A. Methanol usage in toluene methylation with medium and large pore zeolites. *ACS Catal.* **2013**, *3*, 817–825. [CrossRef]
2. Gao, K.; Li, S.; Wang, L.; Wang, W. Study on the alkylation of benzene with methanol to selective formation of toluene and xylene over Co_3O_4-La_2O_3/ZSM-5. *RSC Adv.* **2015**, *5*, 45098–45105. [CrossRef]
3. Liu, C.; Su, J.; Liu, S.; Zhou, H.; Yuan, X.; Ye, Y.; Wang, Y.; Jiao, W.; Zhang, L.; Lu, Y.; et al. Insights into the key factor of zeolite morphology on the selective conversion of syngas to light aromatics over a Cr_2O_3/ZSM-5 catalyst. *ACS Catal.* **2020**, *10*, 15227–15237. [CrossRef]
4. Qian, J.; Xiong, G.; Liu, J.; Liu, C.; Guo, H. A preliminary study on the role of the internal and external surfaces of nano-ZSM-5 zeolite in the alkylation of benzene with methanol. *Ind. Eng. Chem. Res.* **2019**, *58*, 9006–9016. [CrossRef]
5. Wang, X.; Xu, J.; Qi, G.; Li, B.; Wang, C.; Deng, F. Alkylation of benzene with methane over ZnZSM-5 zeolites studied with solid-state NMR spectroscopy. *J. Phys. Chem. C* **2013**, *117*, 4018–4023. [CrossRef]
6. Rakoczy, J.; Romotowski, T. Alkylation of benzene with methanol on zeolites: Infrared spectroscopy studies. *Zeolites* **1993**, *13*, 256–260. [CrossRef]
7. Zhu, Z.; Chen, Q.; Xie, Z.; Yang, W.; Li, C. The roles of acidity and structure of zeolite for catalyzing toluene alkylation with methanol to xylene. *Micropor. Mesopor. Mater.* **2006**, *88*, 16–21. [CrossRef]
8. Hu, H.; Lyu, J.; Rui, J.; Cen, J.; Zhang, Q.; Wang, Q.; Han, W.; Li, X. The effect of Si/Al ratio on the catalytic performance of hierarchical porous ZSM-5 for catalyzing benzene alkylation with methanol. *Catal. Sci. Technol.* **2016**, *6*, 2647–2652. [CrossRef]
9. Hu, H.; Lyu, J.; Cen, J.; Zhang, Q.; Wang, Q.; Han, W.; Rui, J.; Li, X. Promoting effects of MgO and Pd modification on the catalytic performance of hierarchical porous ZSM-5 for catalyzing benzene alkylation with methanol. *RSC Adv.* **2015**, *5*, 63044–63049. [CrossRef]
10. Niziolek, A.M.; Onel, O.; Guzman, Y.A.; Floudas, C.A. Biomass-based production of benzene, toluene, and xylenes via methanol: Process synthesis and deterministic global optimization. *Energy Fuels* **2016**, *30*, 4970–4998. [CrossRef]
11. Zhang, J.; Zhou, A.; Gawande, K.; Li, G.; Shang, S.; Dai, C.; Fan, W.; Han, Y.; Song, C.; Ren, L.; et al. *b*-Axis-oriented ZSM-5 nanosheets for efficient alkylation of benzene with methanol: Synergy of acid sites and diffusion. *ACS Catal.* **2023**, *13*, 3794–3805. [CrossRef]

12. Ren, S.; Tian, C.; Yue, Y.; Zou, W.; Hua, W.; Gao, Z. Selective alkylation of benzene with methanol to toluene and xylene over sheet-like ZSM-5 with controllable *b*-oriented length. *Catal. Lett.* **2023**. [CrossRef]
13. Anderson, J.R.; Mole, T.; Christov, V. Mechanism of some conversions over ZSM-5 catalyst. *J. Catal.* **1980**, *61*, 477–484. [CrossRef]
14. Svelle, S.; Visur, M.; Olsbye, U.; Saepurahman; Bjørgen, M. Mechanistic aspects of the zeolite catalyzed methylation of alkenes and aromatics with methanol: A review. *Top. Catal.* **2011**, *54*, 897–906. [CrossRef]
15. Ivanova, I.I.; Corma, A. Surface species formed and their reactivity during the alkylation of toluene by methanol and dimethyl ether on zeolites as determined by in situ ^{13}C MAS NMR. *J. Phys. Chem. B* **1997**, *101*, 547–551. [CrossRef]
16. Vos, A.M.; Nulens, K.H.L.; De Proft, F.; Schoonheydt, R.A.; Geerlings, P. Reactivity descriptors and rate constants for electrophilic aromatic substitution: Acid zeolite catalyzed methylation of benzene and toluene. *J. Phys. Chem. B* **2002**, *106*, 2026–2034. [CrossRef]
17. Wen, Z.; Zhu, H.; Zhu, X. Density functional theory study of the zeolite-catalyzed methylation of benzene with methanol. *Catal. Lett.* **2019**, *150*, 21–30. [CrossRef]
18. Wen, Z.; Yang, D.; He, X.; Li, Y.; Zhu, X. Methylation of benzene with methanol over HZSM-11 and HZSM-5: A density functional theory study. *J. Mol. Catal. A* **2016**, *424*, 351–357. [CrossRef]
19. Maihom, T.; Boekfa, B.; Sirijaraensre, J.; Nanok, T.; Probst, M.; Limtrakul, J. Reaction mechanisms of the methylation of ethene with methanol and dimethyl ether over H-ZSM-5: An ONIOM study. *J. Phys. Chem. C* **2009**, *113*, 6654–6662. [CrossRef]
20. Van der Mynsbrugge, J.; Visur, M.; Olsbye, U.; Beato, P.; Bjørgen, M.; Van Speybroeck, V.; Svelle, S. Methylation of benzene by methanol: Single-site kinetics over H-ZSM-5 and H-beta zeolite catalysts. *J. Catal.* **2012**, *292*, 201–212. [CrossRef]
21. Kaeding, W.W. Conversion of methanol to hydrocarbons III. Methylation, ethylation, and propylation of benzene with methanol. *J. Catal.* **1988**, *114*, 271–276. [CrossRef]
22. Hu, H.; Lyu, J.; Wang, Q.; Zhang, Q.; Cen, J.; Li, X. Alkylation of benzene with methanol over hierarchical porous ZSM-5: Synergy effects of hydrogen atmosphere and zinc modification. *RSC Adv.* **2015**, *5*, 32679–32684. [CrossRef]
23. Hu, H.; Zhang, Q.; Cen, J.; Li, X. Catalytic activity of Pt modified hierarchical ZSM-5 catalysts in benzene alkylation with methanol. *Catal. Lett.* **2015**, *145*, 715–722. [CrossRef]
24. Khare, R.; Bhan, A. Mechanistic studies of methanol-to-hydrocarbons conversion on diffusion-free MFI samples. *J. Catal.* **2015**, *329*, 218–228. [CrossRef]
25. Liu, S.; Zhang, H.; Chen, H.; Chen, Z.; Zhang, L.; Ren, J.; Wen, X.; Yang, Y.; Li, Y. Fabrication of a core–shell MFI@TON material and its enhanced catalytic performance for toluene alkylation. *Catal. Sci. Technol.* **2020**, *10*, 1281–1291. [CrossRef]
26. Jalil, A.A.; Zolkifli, A.S.; Triwahyono, S.; Rahman, A.F.A.; Ghani, N.N.M.; Hamid, M.Y.S.; Mustapha, F.H.; Izan, S.M.; Nabgan, B.; Ripin, A. Altering dendrimer structure of fibrous-silica-HZSM5 for enhanced product selectivity of benzene methylation. *Ind. Eng. Chem. Res.* **2019**, *58*, 553–562. [CrossRef]
27. Magusin, P.C.M.M.; Zorin, V.E.; Aerts, A.; Houssin, C.J.Y.; Yakovlev, A.L.; Martens, J.A.; van Santen, R.A. Template-aluminosilicate structures at the early stages of zeolite ZSM-5 formation. A combined preparative, solid-state NMR, and computational study. *J. Phys. Chem. B* **2005**, *109*, 22767–22774. [CrossRef]
28. Yokoi, T.; Mochizuki, H.; Namba, S.; Kondo, J.N.; Tatsumi, T. Control of the Al distribution in the framework of ZSM-5 zeolite and its evaluation by solid-state NMR technique and catalytic properties. *J. Phys. Chem. C* **2015**, *119*, 15303–15315. [CrossRef]
29. Pashkova, V.; Sklenak, S.; Klein, P.; Urbanova, M.; Dedecek, J. Location of framework Al atoms in the channels of ZSM-5: Effect of the (hydrothermal) synthesis. *Chem. Eur. J.* **2016**, *22*, 3937–3941. [CrossRef]
30. Dedecek, J.; Balgová, V.; Pashkova, V.; Klein, P.; Wichterlová, B. Synthesis of ZSM-5 zeolites with defined distribution of Al atoms in the framework and multinuclear MAS NMR analysis of the control of Al distribution. *Chem. Mater.* **2012**, *24*, 3231–3239. [CrossRef]
31. Gábová, V.; Dědeček, J.; Čejka, J. Control of Al distribution in ZSM-5 by conditions of zeolite synthesis. *Chem. Commun.* **2003**, *39*, 1196–1197. [CrossRef] [PubMed]
32. Liang, T.; Chen, J.; Qin, Z.; Li, J.; Wang, P.; Wang, S.; Wang, G.; Dong, M.; Fan, W.; Wang, J. Conversion of methanol to olefins over H-ZSM-5 zeolite: Reaction pathway is related to the framework aluminum siting. *ACS Catal.* **2016**, *6*, 7311–7325. [CrossRef]
33. Hur, Y.G.; Kester, P.M.; Nimlos, C.T.; Cho, Y.; Miller, J.T.; Gounder, R. Influence of tetrapropylammonium and ethylenediamine structure-directing agents on the framework Al distribution in B-Al-MFI zeolites. *Ind. Eng. Chem. Res.* **2019**, *58*, 11849–11860. [CrossRef]
34. Biligetu, T.; Wang, Y.; Nishitoba, T.; Otomo, R.; Park, S.; Mochizuki, H.; Kondo, J.N.; Tatsumi, T.; Yokoi, T. Al distribution and catalytic performance of ZSM-5 zeolites synthesized with various alcohols. *J. Catal.* **2017**, *353*, 1–10. [CrossRef]
35. Kim, S.; Park, G.; Woo, M.H.; Kwak, G.; Kim, S.K. Control of hierarchical structure and framework-Al distribution of ZSM-5 via adjusting crystallization temperature and their effects on methanol conversion. *ACS Catal.* **2019**, *9*, 2880–2892. [CrossRef]
36. Al-Nahari, S.; Dib, E.; Cammarano, C.; Saint-Germes, E.; Massiot, D.; Sarou-Kanian, V.; Alonso, B. Impact of mineralizing agents on aluminum distribution and acidity of ZSM-5 zeolites. *Angew. Chem. Int. Ed.* **2023**, *62*, e202217992. [CrossRef] [PubMed]
37. Liu, H.; Wang, H.; Xing, A.; Cheng, J. Effect of Al distribution in MFI framework channels on the catalytic performance of ethane and ethylene aromatization. *J. Phys. Chem. C* **2019**, *123*, 15637–15647. [CrossRef]
38. Wang, S.; Wang, P.; Qin, Z.; Chen, Y.; Dong, M.; Li, J.; Zhang, K.; Liu, P.; Wang, J.; Fan, W. Relation of catalytic performance to the aluminum siting of acidic zeolites in the conversion of methanol to olefins, viewed via a comparison between ZSM-5 and ZSM-11. *ACS Catal.* **2018**, *8*, 5485–5505. [CrossRef]

39. Park, S.; Biligetu, T.; Wang, Y.; Nishitoba, T.; Kondo, J.N.; Yokoi, T. Acidic and catalytic properties of ZSM-5 zeolites with different Al distributions. *Catal. Today* **2018**, *303*, 64–70. [CrossRef]
40. Wang, Y.; He, X.; Yang, F.; Su, Z.; Zhu, X. Control of framework aluminum distribution in MFI channels on the catalytic performance in alkylation of benzene with methanol. *Ind. Eng. Chem. Res.* **2020**, *59*, 13420–13427. [CrossRef]
41. Yue, Y.; Gu, L.; Zhou, Y.; Liu, H.; Yuan, P.; Zhu, H.; Bai, Z.; Bao, X. Template-free synthesis and catalytic applications of microporous and hierarchical ZSM-5 zeolites from natural aluminosilicate minerals. *Ind. Eng. Chem. Res.* **2017**, *56*, 10069–10077. [CrossRef]
42. Sun, Y.; Ma, T.; Cao, S.; Wang, J.; Meng, X.; Gong, Y.; Zhang, Z.; Ma, A.; Liu, P. Defective sites in ZSM-5 zeolite synthesized by n-butylamine template facilitating uniform meso-microporosity by alkali-treatment. *Micropor. Mesopor. Mater.* **2021**, *326*, 11360–11368. [CrossRef]
43. Yang, J.; Gong, K.; Miao, D.; Jiao, F.; Pan, X.; Meng, X.; Xiao, F.; Bao, X. Enhanced aromatic selectivity by the sheet-like ZSM-5 in syngas conversion. *J. Energy Chem.* **2019**, *35*, 44–48. [CrossRef]
44. Wu, D.; Yu, X.; Chen, X.; Yu, G.; Zhang, K.; Qiu, M.; Xue, W.; Yang, C.; Liu, Z.; Sun, Y. Morphology-controlled synthesis of H-type MFI zeolites with unique stacked structures through a one-pot solvent-free strategy. *ChemSusChem* **2019**, *12*, 3871–3877. [CrossRef]
45. Soghrati, E.; Ong, T.K.C.; Poh, C.K.; Kawi, S.; Borgna, A. Zeolite-supported nickel phyllosilicate catalyst for C-O hydrogenolysis of cyclic ethers and polyols. *Appl. Catal. B* **2018**, *235*, 130–142. [CrossRef]
46. Shang, S.; Li, W.; Zhou, A.; Zhang, J.; Yang, H.; Zhang, A.; Guo, X. Fe-Substituted Pt/HZSM-48 for superior selectivity of *i*-C_{12} in *n*-dodecane hydroisomerization. *Ind. Eng. Chem. Res.* **2022**, *61*, 1056–1065. [CrossRef]
47. Parry, E.P. An infrared study of pyridine adsorbed on acidic solids. Characterization of surface acidity. *J. Catal.* **1963**, *2*, 371–379. [CrossRef]
48. Shishido, T.; Hattori, H. Hydrogen effects on cumene cracking over zirconium oxide promoted by sulfate ion and platinum. *J. Catal.* **1996**, *161*, 194–197. [CrossRef]
49. Nie, Y.; Shang, S.; Xu, X.; Hua, W.; Yue, Y.; Gao, Z. In_2O_3-doped Pt/WO_3/ZrO_2 as a novel efficient catalyst for hydroisomerization of n-heptane. *Appl. Catal. A* **2012**, *433–434*, 69–74. [CrossRef]
50. Meng, L.; Zhu, X.; Mezari, B.; Pestman, R.; Wannapakdee, W.; Hensen, E.J.M. On the role of acidity in bulk and nanosheet [T]MFI (T = Al^{3+}, Ga^{3+}, Fe^{3+}, B^{3+}) zeolites in the methanol-to-hydrocarbons reaction. *ChemCatChem* **2017**, *9*, 3942–3954. [CrossRef] [PubMed]
51. Fyfe, C.A.; Gobbi, G.C.; Kennedy, G.J. Investigation of the conversion (dealumination) of ZSM-5 into silicalite by high-resolution solid-state silicon-29 and aluminum-27 MAS NMR spectroscopy. *J. Phys. Chem.* **1984**, *88*, 3248–3253. [CrossRef]
52. Wu, Q.; Liu, X.; Zhu, L.; Ding, L.; Gao, P.; Wang, X.; Pan, S.; Bian, C.; Meng, X.; Xu, J.; et al. Solvent-free synthesis of zeolites from anhydrous starting raw solids. *J. Am. Chem. Soc.* **2015**, *137*, 1052–1055. [CrossRef]
53. Zhu, X.; Wu, L.; Magusin, P.; Mezari, B.; Hensen, E. On the synthesis of highly acidic nanolayered ZSM-5. *J. Catal.* **2015**, *327*, 10–21. [CrossRef]
54. Petushkov, A.; Yoon, S.; Larsen, S.C. Synthesis of hierarchical nanocrystalline ZSM-5 with controlled particle size and mesoporosity. *Micropor. Mesopor. Mater.* **2011**, *137*, 92–100. [CrossRef]
55. Nagy, J.B.; Gabelica, Z.; Debras, G.; Derouane, E.G.; Gilson, J.P.; Jacobs, P.A. ^{27}Al-n.m.r. characterization of natural and synthetic zeolites. *Zeolites* **1984**, *4*, 133–139. [CrossRef]
56. Deng, F.; Du, Y.; Ye, C.; Wang, J.; Ding, T.; Li, H. Acid sites and hydration behavior of dealuminated zeolite HZSM-5: A high-resolution solid state NMR study. *J. Phys. Chem.* **1995**, *99*, 15208–15214. [CrossRef]
57. Blasco, T.; Corma, A.; Martínez-Triguero, J. Hydrothermal stabilization of ZSM-5 catalytic cracking additives by phosphorus addition. *J. Catal.* **2006**, *237*, 267–277. [CrossRef]
58. Saenluang, K.; Imyen, T.; Wannapakdee, W.; Suttipat, D.; Dugkhuntod, P.; Ketkaew, M.; Thivasasith, A.; Wattanakit, C. Hierarchical nanospherical ZSM-5 nanosheets with uniform Al distribution for alkylation of benzene with ethanol. *ACS Appl. Nano Mater.* **2020**, *3*, 3252–3263. [CrossRef]
59. Li, R.; Chawla, A.; Linares, N.; Sutjianto, J.G.; Chapman, K.W.; Martínez, J.G.; Rimer, J.D. Diverse physical states of amorphous precursors in zeolite synthesis. *Ind. Eng. Chem. Res.* **2018**, *57*, 8460–8471. [CrossRef]
60. Jiang, Y.; Hunger, M.; Wang, W. On the reactivity of surface methoxy species in acidic zeolites. *J. Am. Chem. Soc.* **2006**, *128*, 11679–11692. [CrossRef]
61. Svelle, S.; Rønning, P.O.; Kolboe, S. Kinetic studies of zeolite-catalyzed methylation reactions: 1. Coreaction of [^{12}C]ethene and [^{13}C]methanol. *J. Catal.* **2004**, *224*, 115–123. [CrossRef]
62. Svelle, S.; Kolboe, S.; Swang, O.; Olsbye, U. Methylation of alkenes and methylbenzenes by dimethyl ether or methanol on acidic zeolites. *J. Phys. Chem. B* **2005**, *109*, 12874–12878. [CrossRef] [PubMed]
63. Mehio, N.; Dai, S.; Jiang, D.E. Quantum mechanical basis for kinetic diameters of small gaseous molecules. *J. Phys. Chem. A* **2014**, *118*, 1150–1154. [CrossRef] [PubMed]
64. Emeis, C.A. Determination of integrated molar extinction coefficients for infrared absorption bands of pyridine adsorbed on solid acid catalysts. *J. Catal.* **1993**, *141*, 347–354. [CrossRef]

65. Yang, F.; Zhong, J.; Liu, X.; Zhu, X. A novel catalytic alkylation process of syngas with benzene over the cerium modified platinum supported on HZSM-5 zeolite. *Appl. Energy* **2018**, *226*, 22–30. [CrossRef]
66. Frillette, V.J.; Haag, W.O.; Lago, R.M. Catalysis by crystalline aluminosilicates: Characterization of intermediate pore-size zeolites by the "Constraint Index". *J. Catal.* **1981**, *67*, 218–222. [CrossRef]